LRP 451/92 February 1992

THE DYNAMICAL RESPONSE OF THE PLASMA AS A TOOL FOR INVESTIGATING TRANSPORT MECHANISMS

J.-M. Moret, T. Dudok de Wit, B. Joye,
J.B. Lister

submitted to Nuclear Fusion

THE DYNAMICAL RESPONSE OF THE PLASMA AS A TOOL FOR INVESTIGATING TRANSPORT MECHANISMS

J.-M. MORET, T. DUDOK DE WIT, B. JOYE, J.B. LISTER

Centre de recherches en physique des plasmas
Association Euratom - Confédération Suisse
Lausanne, Switzerland

ABSTRACT - The dynamical response of the soft X-ray emission profile to different external perturbations – gas feed, impurity injection, RF power, surface loop voltage – has been studied on the TCA tokamak and analysed using the same techniques. The frequency dependence of the response has been exploited to distinguish between the dominant transport processes. Remarkably similar phase response profiles were obtained with the different stimuli; they show a link with the sawtooth activity. The model which most plausibly explains these experimental observations requires diffusive transport with the diffusive coefficient locally modulated by the perturbation.

CONTENTS

1. INTRODUCTION

Understanding transport mechanisms in tokamak plasmas is important in fusion oriented plasma research since confinement properties are crucial in the design of a future reactor. The poor understanding of even general observations, such as profile consistency, confinement degradation during additional heating or different confinement regimes (L mode, H mode, pellet fuelling) is a justification for the continued effort devoted to this subject.

In a first approach to study tokamak plasma transport, a particle or energy flux balance was generally established from measurements of the radial profiles of plasma parameters in stationary conditions. This approach has several disadvantages : it requires measurements with high spatial resolution and sufficient accuracy to compute the gradients. Another problem is its inability to distinguish concurrent processes such as the energy deposition from additional heating and the subsequent modification of the thermal conductivity.

Another approach, described in this paper, consists of perturbing a few particular parameters which may affect quantities such as the thermal energy or the particle content of the plasma. This gives rise to a temporal evolution (i.e. a dynamical response) of those quantities which is determined by the underlying transport mechanisms. The dynamic response associated with different contending transport models may then be compared to determine which transport mechanisms are the most suitable for describing the experimental observations.

The analysis of the experiments in terms of dynamic response offers many advantages. Firstly, a limited number of experiments is sufficient to get a detailed description of the dynamic response of the plasma parameters. In practice, this implies measurements over a wide range of frequencies and perturbation amplitudes. A second advantage is the availability of well-established signal processing techniques (i.e. Fourier and Laplace transform) which are capable of obtaining high signal-to-noise ratios and extending measurements to domains which remain inaccessible to conventional techniques. Finally, the dynamic response approach offers the advantage that the analysis may be performed without any a priori knowledge of the underlying transport mechanisms. This property makes it more objective and may allow to discover unsuspected aspects of the transport. Based on experimentally established properties of the dynamic response, a model of the transport processes can then be built and validated, giving more confidence in the deduced model than simply adjusting a given

model to fit the temporal evolution of the plasma parameters.

As an illustrative example of this method, consider a quantity y subjected to diffusive transport (y could be for instance the local thermal energy or the local electron density). In a cylinder of radius a, the temporal evolution of y is governed by :

$$\frac{\partial y}{\partial t} = x + \frac{1}{r}\frac{\partial}{\partial r}\left(r\, D\, \frac{\partial y}{\partial r}\right) \qquad (1.1)$$

D is the diffusion coefficient and x the corresponding source term. The following notation will be used: for any given signal u(t), the stationary component is $\langle u \rangle$, the modulated component is $\tilde{u}$ and the complex amplitude of the modulated component is **U**.

A small perturbation $\tilde{x}(t)$ modulated at a frequency $\omega/2\pi$ superposed to a stationary state

$$x(r,t) = \langle x(r) \rangle + \mathbf{X}(r)\, e^{-j\omega t} \qquad (1.2)$$

induces a modulation of the quantity y at the same frequency. Retaining only the perturbed terms of Eq. (1.1) leads to :

$$-j\omega \mathbf{Y} = \mathbf{X} + \frac{1}{r}\frac{\partial}{\partial r}\left(r\, D\, \frac{\partial \mathbf{Y}}{\partial r}\right) \qquad (1.3)$$

Without any loss of generality the phase reference can be chosen such that **X** is real and the real and imaginary parts of (1.3) may then be separately expressed as

$$\omega\, Im(\mathbf{Y}) = \mathbf{X} + \frac{1}{r}\frac{\partial}{\partial r}\left(r\, D\, \frac{\partial Re(\mathbf{Y})}{\partial r}\right) \qquad (1.4)$$

$$-\omega\, Re(\mathbf{Y}) = \frac{1}{r}\frac{\partial}{\partial r}\left(r\, D\, \frac{\partial Im(\mathbf{Y})}{\partial r}\right) \qquad (1.5)$$

This gives a set of two non-complex equations from which, if **Y** is known, the radial profiles of **X** and D can be obtained. The left hand side of Eq. (1.3), which vanishes for stationary conditions, yields the missing information required for evaluating these two profiles simultaneously. Repeating the experiment at different frequencies should not alter the results, otherwise the model as expressed by Eq. (1.1) is not correct and must be modified. Thus the frequency dependence of the dynamic response provides information for validating a given model. For example, when using a frequency much higher than the inverse

characteristic confinement time (i.e. when ω exceeds D/a^2), Eq. (1.3) reduces to

$$-j\omega \mathbf{Y} \cong \mathbf{X} \tag{1.6}$$

In this case, the absorbed energy or the particles hardly leave the source region within one modulation cycle, leading to a perturbation localised in the deposition region. The complex amplitude of $\mathbf{Y}$ ought then to be in quadrature with the external perturbation (i.e. $\mathbf{Y}$ has a phase lag of 90° with respect to $\mathbf{X}$) and its modulus should decrease as the inverse of the modulation frequency. These properties of the transfer function can be verified experimentally.

This example illustrates how a dynamical approach can extract information which would be either difficult or impossible to obtain in stationary conditions. This approach has been used to study different transport processes such as particle transport with the gas feed as stimulus [1-3], heat transport with RF power modulation [4-9] and heat and particle transport due to internal disruptions [10-12]. It should be noted that most of these experiments have made little or no use of the frequency dependence of the dynamical response of the measured parameters. The interpretation and usefulness of this frequency dependence is treated in detail in this paper, when analysing the experimental data.

On TCA, the initial aim was to study the response of the soft X-ray emission to Alfvén wave heating power modulation to reveal features of the RF power deposition profile [7]. Initial experiments showed quite unsuspected response profiles and this incited to extend the method to other stimuli such as perturbations of the electron density, the impurity influx or the surface loop voltage. A wide range of conditions has been explored, in which mainly the dynamical response of the soft X-ray emission and that of the electron density were studied. The aim of this paper is to present a synthesis of these experiments. A rather qualitative approach will be adopted which allows to discard some of the conventional models used for transport and help build a coherent picture of the plasma response. The main goal is thus to provide a solid description of some of the simple properties which any transport model must possess if it is to explain transport in a tokamak plasma. The observed properties should also stimulate the invention or completion of models which agree with the observed behaviour.

The outline of the paper is as follows : in Section 2 the diagnostics used in the experiments are presented. Section 3 describes the analysis techniques. The dynamical response of the soft X-ray emission profile to a modulation of the density induced by gas puffing is presented in Section 4. Section 5 recalls the main observations made with Alfvén wave power modulation experiments.

Section 6 and 7 are dedicated to two other stimuli which affect the plasma : impurity injection and surface loop voltage modulation. In Section 8, the decomposition of the soft X-ray emission en terms of electron temperature and density is discussed. On the basis of these results, a model of the dominant transport mechanism is proposed in Section 9. In Section 10, the implications of this model are discussed.

2. EXPERIMENTAL CONDITIONS

The experiments described in this paper were carried out in deuterium discharges in the TCA tokamak with the following parameters :

major radius R = 0.61 m
minor radius a = 0.18 m
toroidal magnetic field : 1.5 T
plasma current : $40 < I_p < 130$ kA
line average density : $1 < \overline{n}_e < 5 \cdot 10^{19}$ m^{-3}
central electron temperature : $0.3 < T_{eo} < 1$ keV

The additional heating was provided by Alfvén waves launched by 8 phase coherent antennae at frequencies $2 < f < 5$ MHz. The Alfvén wave excitation and heating experiments are described in [13,14].

The main diagnostics used in this work are a 15 channel soft X-ray pin-hole camera viewing the plasma horizontally from $r/a = -0.68$ to 0.79 and a 4 channel FIR (λ=447μm) interferometer with chords located at $r/a = -0.56$, -0.11, 0.33 and 0.89. The soft X-ray emission will hereafter be referred to as the emission. It depends on the electron temperature, the impurity density, the electron density and a correction for the impurity concentration which may be described by :

$$A = f(Z_{eff}, Z_I) \cdot n_I \cdot n_e \cdot T_e^{\alpha} \qquad (2.1)$$

For a plasma in which the impurity concentration is constant ($n_I \sim n_e$) and for small perturbations, the normalised modulation can be decomposed as :

$$\frac{\mathbf{A}}{\langle A \rangle} = \frac{\mathbf{f}}{\langle f \rangle} + \alpha \frac{\mathbf{T_e}}{\langle T_e \rangle} + 2 \frac{\mathbf{n_e}}{\langle n_e \rangle} \qquad (2.2)$$

The temperature-dependent exponent α varies between 1.5 at the centre and 6 for the outermost camera channel. Since the relative modulation amplitudes of the density, the electron temperature and the impurity concentration can be of similar magnitude, nothing will be said a priori about the term which dominates in Eq. (2.2), although the emission near the edge can be expected to be mostly sensitive to temperature changes. The dynamical response analysis will help separate the contribution from each of these terms.

3. ANALYSIS METHODS

The dynamical response of the plasma is studied by applying a perturbation and measuring the reaction. If the response is linear, the dynamical response may be expressed by its linear transfer function $\mathbf{H}(\omega)$, defined as the complex ratio between the modulated component of the response signal **Y**, and the modulated input signal **X** at a given frequency $\omega/2\pi$:

$$\mathbf{H}(\omega) = \frac{\mathbf{Y}}{\mathbf{X}} \tag{3.1}$$

This transfer function is usually expressed by its modulus or gain $|\mathbf{H}(\omega)|$ and its argument or phase $\angle\mathbf{H}(\omega)$. Two techniques, described in the appendix, were used to obtain the transfer function.

1) When the perturbation waveform is externally controllable, as is the case with gas feed, RF power or surface loop voltage modulation, a sinusoidal excitation was chosen. The modulated components of the signals were then extracted using a modification of the Fourier technique which gives improved time resolution and noise rejection, and the ability to work in transient conditions. However, to obtain a complete picture of the transfer function, the experiment must be repeated at several modulation frequencies, which requires a considerable experimental investment.

2) When the perturbation waveform is not controllable as in the case of laser-injected impurities, or when a non-sinusoidal input signal is chosen, a system identification analysis is used. This method gives the transfer function over a continuous frequency range. It extracts much more information from a single plasma discharge, the major drawbacks being a limited time resolution and a lower signal-to-noise ratio.

These two techniques give results in excellent agreement. In practice, the modulation frequency is limited on the low side by the duration of the discharge. An upper limit is set by the sawtooth activity and by the signal-to-noise ratio, which inevitably decreases at high frequencies. In our experiments, this frequency range is 30 to 600 Hz which corresponds to a timescale range which covers the global electron confinement time ($\tau_{Ee} \leq 10$ ms).

The linearity of the response has to be verified for each experiment. When a sinusoidal excitation is used, the absence of harmonics of the modulation frequency may be used as proof of the linearity. The independence of the

A plasma density scan showed that neither the absolute phase of the perturbed emission nor that of the perturbed electron density change significantly with $\overline{n}_e$, the line-averaged plasma density. The characteristic time constants of the emission are thus independent of the density whereas the relative amplitudes of the perturbed emission, decrease as $\overline{n}_e$ increases with a scaling :

$$\frac{|A|}{\langle A \rangle} \sim \omega^{-2} \overline{n}_e^{-2} \tag{4.1}$$

for all the chords. The quadratic dependence on ω suggests that the perturbed emission is a more complicated function of the source than expressed in Eq. (1.1). This indicates the presence of an intermediate transport mechanism, and will be further discussed in section 10.

4. DYNAMICAL RESPONSE TO GAS FEED MODULATION

The average plasma density has early been identified as an important quantity in the parameterisation of the confinement time. Recently, different density profiles obtained by pellet injection, gas puffing or neutral beam heating have also been shown to have a considerable effect on the confinement properties of the plasma [16]. This suggests that the temporal evolution of the plasma parameters following a modification of the plasma density or of its profile may reveal aspects of the underlying transport mechanisms.

On TCA, the dynamical response of the emission to the plasma density was measured by sinusoidally modulating the gas feed at frequencies ranging from 30 to 300 Hz. The raw emission and the line-averaged electron density during such an experiment performed at 100 Hz are shown in Fig. 1. The same figure also shows the relative modulated component of each quantity $\tilde{A}/\langle A \rangle$.

Figure 2 shows the radial profile of the transfer function between the line-averaged density and the emission expressed as a relative gain and phase for two values of the plasma current. The phase is chosen such that a positive value corresponds to a delay. Since the phase must evolve continuously as the frequency increases from zero it can be fixed absolutely. The experiments have been performed with sufficiently small frequency steps, guaranteeing that the ± 180° ambiguity has been resolved and the phase in Fig. 2 is correct.

The observed response profiles are divided into two distinct regions separated by a well defined radius. Inside this radius, both the phase and the gain are lowest and fairly flat whereas, outside this region, they both increase with a sharp jump. The separation between the two regions was found to be closely related to the sawtooth inversion radius. Figure 3 shows the results of plasma current scan which changes the q=1 radius indicating that these radii move together. In this figure, the sawtooth inversion radius was obtained from the Abel-inverted emission profiles and the q=1 radius measured by phase contrast interferometry [17]. The flatness of the phase profile inside the q=1 radius for all the modulation frequencies used indicates that the transport processes inside this radius are much faster than outside. This can be seen as the consequence of sawtooth mixing since the modulation frequency was always smaller than the sawtooth frequency. In the absence of sawtooth activity, typically for q(a) > 6, this picture changes : the discontinuity in the phase and amplitude profiles disappears and the phase profile becomes smooth, with a minimum at the plasma centre.

measured transfer function to the amplitude of the excitation was also confirmed. These conditions were found to be satisfied for small modulation amplitudes ($0 < |A|/\langle A \rangle < 20$ % for the emission) in the specified frequency range [15].

5. DYNAMICAL RESPONSE TO ALFVEN WAVE HEATING

The Alfvén power deposition profile has been studied by measuring the plasma dynamic response to RF heating power. The soft X-ray emission results have already been reported in [18], and the ion thermal energy modulation in [19]. In this section, the salient points are recalled and related to the observations made in the previous sections.

To measure the dynamical response of the parameters to RF power modulation, both experimental procedures described in Section 3 were used. In the first case, the RF power was modulated sinusoidally at frequencies in the range 30—600 Hz and in the second procedure, the dynamical response to a change in the RF power was used to identify the transfer function, Fig. 4c.

The radial profile of the relative gain and of the phase of the emission response to a sinusoidal modulation of the RF power is shown in Fig. 5 for two modulation frequencies. All the characteristics of the response observed during gas feed modulation, Fig. 2, reappear in these profiles. An unexpected result is the high value of the phase which increases with frequency and does not saturate at 90° as would be expected for a direct heat deposition. The characteristic time constant of the response is again smaller at high plasma current, as observed for the density modulation.

The emission response to RF power can be compared not only qualitatively but also quantitatively with the gas feed modulation. To accomplish this, the phases must be measured with respect to a common reference. Choosing the line-averaged density as the phase reference, both the RF power modulation and the gas feed modulation provided the same absolute phase profiles, Fig. 6. The ratios between the central emission amplitude and the relative density amplitude were also similar, Fig. 7. The emission response observed during Alfvén wave heating is concluded to be mostly due to a more basic response of the plasma to a change in the density, which can also be produced with gas puffing. The larger effect during the RF heating is due to the higher rate of change of the density during RF heating than was achievable with gas puffing.

A consequence of the predominant effect of the density on the emission response is a lack of sensitivity of this response to the position of the Alfvén resonance layers [15]. Figure 8 shows an experiment in which the resonant radial structure was modified by a small change in the RF frequency. At lower density or RF frequency, the Alfvén resonance layers are located in the plasma periphery. A

small increase in the density or the RF frequency will create a new resonance layer into the plasma centre, leading to an increased RF power deposition at the plasma centre. The phase was not significantly affected, apart from an additional delay after the arrival of a new resonance layer. Despite the large experimental error bars, the relative amplitude of the emission perturbation is seen to decrease by a factor of 2 throughout the plasma volume when a new resonance appears at the plasma centre and when the RF power is expected to be deposited towards the plasma edge. This observation must be related to simultaneous discontinuities observed on the time evolution of several macroscopic parameters such as the internal inductance l_i and the sawtooth period [14] when the resonance layer moves outwards.

The dynamical response analysis highlights the dominant effect of the density rise associated with RF power. Although the density rise leads to a global energy increase, it remains difficult to determine any direct electron heating. Experiments were performed to reduce the density-related effects by gas feed and RF power countermodulation [20] adjusting the relative amplitudes and phases of both perturbations to obtain a minimal modulation of the density, achieving below 1% throughout the plasma volume. The response profiles measured during these discharges were not significantly modified, Fig. 9. The emission modulation at the plasma centre was halved showing that a sizeable component of the modulated emission is due to a direct effect of the wavefield.

6. DYNAMICAL RESPONSE TO THE INJECTION OF IMPURITIES

Impurity injection is a technique used to investigate the ion confinement properties in a tokamak [21,22]. In this section, the temporal evolution of the emission following the injection of aluminium into the plasma is analysed.

The impurity injection is produced by laser ablation of a 0.2 μm layer of aluminium evaporated on a glass plate. The total number of ablated atoms is of the order of $3 \cdot 10^{16}$, leading to an increase of the plasma density of less than 0.2 %. During this experiment, the thickness of the Beryllium filter between the plasma and the soft X ray diodes was increased from 25 to 250 μm, strongly reducing the contribution from aluminium line-emission to the measured emission. Since the density variation was well below the emission excursion, Fig. 4b, the emission perturbation may be ascribed to a change of either the electron temperature or the concentration of higher Z impurities.

Immediately after impurity injection, the central region of the plasma shows a uniform emission increase, Fig. 4b. Outside a well defined radius, the emission initially decreases, and then increases due to the outward propagation of the initial perturbation. A scan of the plasma current again shows that this discontinuity occurs just outside the sawtooth inversion radius. Moreover, the time constants of the dynamical response are larger at low current, which was also observed with density and RF power modulation. This behaviour of the emission is similar to the reaction of the plasma to a short gas puff or a RF power pulse, shown in Fig. 4a and 4c respectively.

A fuller analysis was carried out by estimating the transfer function between the emission response and the impurity injection with the system identification technique described in the appendix, using the impurity injection time to fix the phase reference. The phase and the gain response profiles were extracted as a function of frequency from a single experiment, and were found to be strikingly similar to those obtained by sinusoidal gas feed modulation which also had a discontinuity at the q=1 radius, Fig. 10. This resemblance reveals the existence of a common transport process, which is similar for impurity ion and electron transport.

7. DYNAMICAL RESPONSE TO SURFACE LOOP VOLTAGE MODULATION

Another way to affect the energy content of the plasma is to modify the ohmic power deposition by changing the plasma surface loop voltage. This experiment was performed by adding small perturbations to the surface loop voltage [15] which resulted in an inward propagating perturbation of the emission, Fig. 11. Since there is no significant change in the electron density, this is attributed to a modification of the electron temperature.

The results were simulated using a linearized model of heat and current transport with neoclassical conductivity and measured temperature profiles. The simulation shows that the effect of the loop voltage modulation is a current perturbation generated at the plasma edge which gradually converts into a heat pulse as it propagates inwards. Given the good agreement between simulated and the experimental results, it was investigated whether a comparison between model and experiment could provide additional information on the current or heat transport processes. Unfortunately, for these experiments the heat source is not separable as in Eq. (1.2), but propagates both in space and time. Practically, this appears as a coupling between the heat and the current transport, which complicates the interpretation of the response profiles. A separate quantification of the transport mechanisms is still possible, but only if the two processes have sufficiently different time-scales.

The gradient of the temperature phase profile versus the heat diffusion coefficient χ_e can be used to illustrate the coupling between heat and current transport. In a source-free region of the plasma and for a given modulation frequency, the gradient of the phase profile is only a function of the local value of χ_e (see section 9). The two parameters are plotted in Fig. 12 for different values of the characteristic current diffusion coefficient given as $D_j = \eta_\perp/\mu_o$, where $\eta_\perp$ is the perpendicular resistivity. When $\chi_e << D_j$, the ohmic heat source propagates faster than the heat it generates, and the gradient is determined by the value of D_j. When $\chi_e >> D_j$ the opposite occurs, and the gradient is mainly a function of χ_e. For the plasma parameters encountered in TCA, the heat and current diffusion coefficients obtained in the confinement region are of similar magnitude. Thus the phase gradient is a function of both χ_e and D_j, which prohibits further use of the emission response in diagnosing the heat or current transport.

In conclusion, the phase profiles of the dynamical response to the surface loop voltage differ completely from those observed with gas valve or RF power modulation. Thus, they cannot be explained by the same change in the Poynting

vector at the edge cannot as with gas or impurity injection, or RF power modulation. It must however be pointed out that all the different phase profiles were flat inside the inversion radius, which indicates that the transport in this region is fast.

8. PARAMETRIC DEPENDENCE OF THE SOFT X-RAY EMISSION

The perturbed emission can be expressed as the sum of several plasma parameters, Eq. (2.2). This prohibits any direct interpretation of the emission response in terms of heat or particle transport. To isolate the contributions from the different parameters, the response profiles to different stimuli are compared, and additional diagnostics are used in addition to the soft X-ray camera : the FIR interferometer, providing the electron density with good temporal but limited radial resolution, and a 10-channel Thomson scattering diagnostic, yielding both the electron temperature and density for a single time in the discharge. The latter was fired a different times for 25 similar discharges with a 70 Hz RF power modulation to obtain a temporal evolution.

In all the experiments with a density change, the interferometer shows an inward propagating density perturbation, consistent with the transport of particles injected from the plasma edge. Outside a radius corresponding to the q=1 surface, the density and emission perturbations move in opposite directions. Inside this radius, the phase profiles are identical (Fig. 13) and a non negligible modulation of the central electron density is observed. This can be quantified by the ratio of the relative amplitudes, measured at the plasma centre :

$$\left|\frac{\mathbf{A}}{\langle A\rangle}\right| \Big/ \left|\frac{\mathbf{n_e}}{\langle n_e\rangle}\right| \gtrsim 2 \qquad (8.1)$$

This amplitude ratio suggests that changes in the central emission are linked to changes in the central density. An upper bound for the relative temperature modulation is provided by Thomson scattering data which at all radii give

$$\left|\frac{\mathbf{T_e}}{\langle T_e\rangle}\right| \lesssim 0.7 \left|\frac{\mathbf{n_e}}{\langle n_e\rangle}\right| \qquad \text{at all r} \qquad (8.2)$$

The perturbed electron density component can be cancelled by suitably countermodulating the gas feed and the RF power. As expected, this causes a reduction in the emission modulation amplitude. The phase profile however, is not significantly affected. In particular, the characteristic phase jump is still observed. Hence, even if the electron density contributes to the dynamic response of the emission, it is insufficient to explain the response profile outside

the q=1 radius.

According to Eq. (2.2), temporal changes in the impurity concentration contribute to the dynamic response of the emission. To assess this affect, the RF power modulation experiments were repeated after the tokamak vacuum vessel had been boronised [23]. The effect of the boronisation was a large reduction in the impurity concentration and the disappearance of heavy impurities; the emission profile peaked and its amplitude dropped by a factor of 100, thereafter recovering on a timescale of a few hundred discharges. In such clean discharges, the lower amplitude ratio of Eq. (8.1) was measured. Its value is consistent with an impurity concentration which remains constant in time. The absolute phase with respect to the stimulus changed little (Fig. 9) indicating that the time constants are independent of the impurity concentration.

When operating both in a clean plasma and with gas feed and RF power countermodulation, the contributions from electron density and impurity concentration modulation are minimised. Under these conditions, the emission still shows a significant residual modulation, which is attributed to the electron temperature. The resulting phase profile again is flatter than under standard conditions, but its characteristic features remain the same, Fig. 9. This suggests that these features can be explained both by the particle density and by the electron temperature. The emission becomes increasingly sensitive on the temperature near the plasma edge, since the calculated temperature exponent α given in Eq. (2.2) rises from approximately 2 at the q=1 radius to 6 near the edge. This temperature sensitivity of the emission was further checked by changing the thickness of the Beryllium filter in the pinhole camera from 25μm to 250μm, which increased α by approximately 1.9 and indeed resulted in a larger amplitude ratio.

In conclusion, all the plasma parameters appearing in Eq. 2.2 contribute to the modulation of the emission. In most experiments, their relative modulation amplitudes are similar, which prohibits them from being clearly separated. However, the response profile of the emission turns out to be quite insensitive to the kind of plasma parameter which is preferentially modulated. Hence, the dynamic response of the emission reveals that the underlying mechanisms could be common for both particle and heat transport. This property will allow us to use a common treatment without having to refer explicitly to either of the transported quantities.

9. MODELLING OF THE TRANSPORT MECHANISMS

The frequency dependence can be used to provide additional information on the underlying transport processes. A diffusive and a convective transport model are examined, and the resulting dynamical response calculated. Any plasma parameter y(r,t) on which the emission depends can be considered, such as the electron temperature, electron density, impurity concentration etc.

If the transport is dominated by convection, then

$$\frac{\partial y(r,t)}{\partial t} = -\frac{1}{r}\frac{\partial}{\partial r}(r\,v\,y) + x(r,t) \tag{9.1}$$

where v is the drift velocity and x is the energy or particle source term. In the source-free region of the plasma, Eq. (9.1) reduces to

$$-j\,\omega\,\mathbf{Y} = -\frac{1}{r}\frac{\partial}{\partial r}(r\,v\,\mathbf{Y}) \tag{9.2}$$

which can be integrated to give

$$\mathbf{Y} = \frac{\mathbf{c}}{r\,v}\,e^{j\omega\,\tau(r)} \tag{9.3}$$

where

$$\tau(r) = \int_0^r \frac{dr'}{v} \tag{9.4}$$

and the complex integration constant **c** is determined by the boundary conditions. The phase is a linear function of the modulation frequency

$$\angle\mathbf{Y} = \angle\mathbf{c} + \omega\tau \tag{9.5}$$

since in the presence of convection, a perturbation propagates with a pure time delay.

If the transport is dominated by diffusive processes, then

$$\frac{\partial y(r,t)}{\partial t} = \frac{1}{r}\frac{\partial}{\partial r}\left(r\,D\,\frac{\partial y}{\partial r}\right) + x(r,t) \tag{9.6}$$

so that the modulated loss term becomes

$$- j\omega \mathbf{Y} = \frac{1}{r}\frac{\partial}{\partial r}\left(r D \frac{\partial \mathbf{Y}}{\partial r}\right) \tag{9.7}$$

With a spatially uniform diffusion coefficient, the solution of this equation is a linear combination of Bessel functions

$$\mathbf{Y} = \mathbf{c}_1 J_0(\mathbf{k}r) + \mathbf{c}_2 N_0(\mathbf{k}r) \tag{9.8}$$

whose argument is

$$\mathbf{k}\, r = -\sqrt{\frac{j\omega r^2}{D}} \tag{9.9}$$

The two integration constants $\mathbf{c}_1$ and $\mathbf{c}_2$ are again determined by the boundary conditions. When $|\mathbf{k}r| \gtrsim 1$, i.e. when $\omega \gtrsim D/r^2$, the asymptotic behaviour of the Bessel functions can be used and the phase of the perturbation becomes

$$\angle \mathbf{Y} = \angle \mathbf{c} + \sqrt{\frac{\omega r^2}{2D}} \tag{9.10}$$

where $\mathbf{c}$ is a complex constant. In the case of heat diffusion, the resulting electron temperature phase would be

$$\angle \mathbf{T}_e = \angle \mathbf{c} + \sqrt{\frac{3}{4}\frac{\omega r^2}{\chi_e}} \tag{9.11}$$

It is important to note that if a radial dependence of the diffusion equation is included, only the radial dependence of the phase is affected, not the frequency dependence.

A comparison of Eq. (9.5) and Eq. (9.11) illustrates how the frequency dependence of the dynamical response contains information about the dominant transport mechanisms. Provided that the modulation frequency is larger than the characteristic confinement time, extended measurements of the phase allow a discrimination between convection and diffusion. On TCA, the best agreement was obtained with the diffusive model, seen in Fig. 14 where the phase of the emission at different radii is plotted as a function of the square root of the modulation frequency. On the basis of this comparison, any major contribution from convective transport during non stationary regimes can be discarded and the relaxation of the emission perturbation must be governed by a diffusive process. The spatial dependence of the results must be used to estimate the diffusion coefficient, and a solution which agrees both in ω and r domains must be sought.

10. DISCUSSION

The two characteristic features of the response profile are the local minimum at the q=1 radius and the large phase jump which occurs just outside it. A local phase increase is generally interpreted as a slowing down of a perturbation, which may result from a local transport barrier. An insulating barrier at the inversion radius was observed in TFR where the cold wave produced by pellet injection slowed down upon reaching the q=1 surface [24], and in PLT by studying impurity transport following laser ablation [21]. The existence of such a transport barrier on TCA can be verified by measuring the frequency dependence of the phase jump, which should increase with the square root of the modulation frequency. Such a dependence was not observed, as the phase jump saturates at ~180° at the highest frequencies. Thus, a local reduction in the heat or the particle flow is not sufficient to explain the measured response profiles and a better model must be sought.

Given the dominant role played by diffusion, the possibility that the diffusion coefficient itself is modulated is considered

$$D(r,t) = \langle D(r) \rangle + \mathbf{D}(r)\, e^{-j\omega t} \tag{10.1}$$

Such a variation of the thermal diffusion coefficient was suggested on TFR to explain the time delay between an ECRH power step and the induced temperature rise [25]. Substituting Eq. (10.1) into Eq. (9.6) and retaining only the dominant terms which are first order in the perturbation amplitude, the particle or power balance becomes

$$-j\omega \mathbf{Y} = \frac{1}{r}\frac{\partial}{\partial r}\left(r \langle D \rangle \frac{\partial \mathbf{Y}}{\partial r}\right) + \frac{1}{r}\frac{\partial}{\partial r}\left(r \mathbf{D} \frac{\partial \langle y \rangle}{\partial r}\right) \tag{10.2}$$

The new term appears as an effective particle or energy source

$$\mathbf{X}^{*} = \frac{1}{r}\frac{\partial}{\partial r}\left(r \mathbf{D} \frac{\partial \langle y \rangle}{\partial r}\right) \tag{10.3}$$

A localised perturbation of D gives rise to a source dipole with positive and negative components. Its effect on the electron temperature is very similar to that of the energy release following an internal disruption, Fig. 15. At high modulation frequencies, two source peaks drive the modulation in quadrature and in antiphase on each side of the region where the diffusivity is affected which results in the observed phase jump.

This model was refined by adjusting the profiles of D and $\tilde{D}$ until the frequency dependence of the calculated response profiles was in agreement with the experimental results. To simulate the enhanced transport inside the q=1 radius, the value of D was increased inside this radius. The estimation of D and $\tilde{D}$ from the measured response profiles is a difficult problem which generally does not have a well defined solution. Nevertheless, a strong similarity is observed for the models which best reproduce the measured response and which have in common a $\tilde{D}$ perturbation which is small except at the transition region between enhanced and reduced transport, Fig. 16. Such a local perturbation of the diffusion coefficient is sufficient to reproduce both the local phase minimum and the phase jump occurring just outside it.

A simple explanation of the observed response has been found on the basis of a local modulation of the diffusion coefficient at the q=1 radius. This returns the discussion to the role played by internal disruptions. Sawtooth activity cannot be simply interpreted in terms of continuous diffusive and convective transport equations; nevertheless its effect on the plasma is often modelled as an insulating barrier which opens periodically at each internal disruption [10]. In this analysis of the dynamical response, such a mechanism will be averaged over several sawtooth periods. The observed similarities and the derived models suggest that the dynamical response of the emission can be explained in terms of the quantity of heat or particles transported across the q=1 surface during a sawtooth crash. A more detailed analysis of the sawtooth parameters has indeed revealed that the sawtooth period and crash amplitude are also modulated during our experiments [26].

What causes the diffusivity to be modulated by external perturbations remains to be determined. All the experiments provide a stimulus which modifies the edge plasma conditions by the injection of the working gas, by an influx of intrinsic impurities, by a high-Z impurity injection or by the presence of Alfvén resonance layers near the plasma edge. The phase response profiles associated with these different stimuli all show that the emission perturbation starts as the incoming particle flux arrives at the q=1 surface. Thus the dynamical response of the emission is the consequence of two succesive mechanisms : in a first stage, an inward propagating density perturbation is created at the plasma edge. When this perturbation reaches the q=1 surface, it affects the sawtooth parameters. This appears as a local change in the diffusion coefficient profile, which in a second stage gives rise to the characteristic emission response profile.

This model successfully reproduces most of the features of the plasma behaviour.

In particular, it provides an explanation for the quadratic dependence in Eq. (4.1), which suggested the presence of an intermediate mechanism. Yet it must be stressed that additional effects could exist during our experiments. There may remain a small direct electron heating by Alfvén waves in the RF experiments; current profile changes may occur during the temperature drop at the plasma edge, resulting in a peaking of the current profile and an increased ohmic power deposition at the centre of the plasma. Such mechanisms may exist in our experiments, but they are certainly not dominant since alone they can not explain the observed response. In particular, they would fail to explain the heat pulse following the initial temperature drop, and the time constants involved with current diffusion are too long to agree with the measured phase profiles.

11. CONCLUSION

The aim of the work presented in this paper was the investigation of the basic transport processes by means of the dynamical response of the soft X-ray emission to many different perturbations: gas feed, RF power and surface loop voltage modulation, and impurity injection. These experiments were performed in the same conditions and analysed using the same techniques, in order to be compared. All the stimuli, except the surface loop voltage, gave remarkably similar response profiles with a discontinuity near the q=1 radius. The frequency dependence of the response was exploited to distinguish between transport mechanisms. The soft X-ray emission profile relaxation was concluded to be governed by a diffusive process and any effects due to convection are negligible. Furthermore, the discontinuity in the phase profile cannot be attributed to a transport barrier. A plausible model is obtained by allowing the diffusion coefficient to be locally modulated at the q=1 radius, which is consistent with the effect of the sawtooth activity. This modulation appears to be triggered by changes in the local particle profile.

These conclusions have been drawn independently of any assumptions on the origin of the response of the soft X-ray emission. In most experiments, the response can be ascribed to a simultaneous modulation of the electron density, the impurity concentration and the electron temperature, thereby prohibiting any direct interpretation in terms of heat or particle transport. But when any of these plasma parameters is predominantly modulated, the response profile is hardly affected. This suggests that the modulation of the diffusion coefficient is common to both heat and particle transport mechanisms.

ACKNOWLEDGEMENTS : We would like to acknowledge stimulating discussions with Dr. A. Bondeson and thank the members of the TCA team for their assistance. Ch. Nieswand provided the the FIR interferometer data and Dr. Z.A. Pietrzyk provided the Thomson scattering data. This work was partly funded by the Fonds National Suisse de la Recherche Scientifique.

REFERENCES

[1] BAGDASAROV, A.A., VASIN, N.L., VERSHKOV, V.A., et al., in Plasma Physics and Controlled Nuclear Fusion Research 1984 (Proc. 10th Int. Conf., 1984, London), Vol. 1, IAEA, Vienna (1985) 181.

[2] GENTLE, K.W., RICHARDS, B., WAELBROECK, F., Plasma Phys. Controll. Fusion **29** (1987) 1077.

[3] KRIEGER, K., FUSSMANN, G, Nucl. Fus. **30** (1990) 2392.

[4] JAHNS, G.L., WONG, S.K., Prater, R., LIN, S.H., EJIMA, S., Nucl. Fus. **26** (1986) 226.

[5] HARTFUSS, H.J., MAASSBERG, H., TUTTER, M., W VII A team, Nucl. Fus. **26** (1986) 678.

[6] ALIKAEV, V., BAGDASAROV, A., BEREZVSKII, E., et al., Plasma Phys. Controll. Fusion **29** (1987) 1285.

[7] JOYE, B., LISTER, J.B., MORET, J.-M., in Controlled Fusion and Plasma Physics (Proc. 14th Europ. Conf., Madrid 1987), Vol. 3, European Physical Society (1987) 950.

[8] ASHRAF, M., BISHOP, C.M., CONNOR, J.W., et al., in Plasma Physics and Controlled Nuclear Fusion Research 1988 (Proc. 12th Int. Conf., Nice, 1988), Vol. 1, IAEA, Vienna (1989) 275.

[9] LEBEAU, D., KOCH, R., MESSIAEN, A. M., et al, Plasma Phys. Controll. Fusion **32** (1990) 249.

[10] JAHNS, G.L., SOLER, M., WADDELL, B.V., et al, Nucl. Fus. **18** (1978) 609.

[11] TARONI, A., TIBONE, F., in Controlled Fusion and Plasma Physics (Proc. 14th Europ. Conf., Madrid 1987), Vol. 1, European Physical Society (1987) 97.

[12] LOPES CARDOZO, N.J., DE HAAS, J.C.M., HOGEWEIJ, G.M.D. et al., Plasma Phys. Controll. Fusion **32** (1990) 983.

[13] COLLINS, G.A., HOFMANN, F., JOYE, B., et al., Physics Fluids **29** (1986) 2260.

[14] BESSON, G., DE CHAMBRIER, A., COLLINS, G.A., et al., Plasma Phys. Controll. Fusion **28** (1986) 1291.

[15] MORET, J.-M., Etude de la réponse dynamique du plasma de TCA et ses conséquences sur la compréhension du confinement et du chauffage, PhD thesis n°758, EPFL, Lausanne (1988).

[16] GRUBER, O., FAHRBACH, H.U., GEHRE, O., et al., Plasma Phys. Controll. Fusion **30** (1988) 1611.

[17] WEISEN, H., BORG, G., JOYE, B., KNIGHT, A.J., LISTER, J.B., Phys. Rev. Lett **62** (1989) 434.

[18] JOYE, B., LISTER, J.B., MORET, J.-M., POCHELON, A. and SIMM, C.W.,

Plasma Phys. Controll. Fusion **30** (1988) 743.

[19] DE CHAMBRIER, A., DUVAL, B.P., LISTER, J.B., et al., Plasma Phys. Controll. Fusion **31** (1989) 527.

[20] DUDOK DE WIT, T., JOYE, B., LISTER, J.B., et al., in Controlled Fusion and Plasma Physics (Proc. 16th Europ. Conf., Venice 1989), Vol. 3, European Physical Society (1989) 1195.

[21] COMPANT LA FONTAINE, A., DUBOIS, M.A., PECQUET, A.L., et al., Plasma Phys. Controll. Fusion **27** (1985) 229.

[22] HAWKES, N., WANG, T., BARNSLEY, R., et al., in Controlled Fusion and Plasma Physics (Proc. 16th Europ. Conf., Venice 1989), Vol. 1, European Physical Society (1989) 79.

[23] DUDOK DE WIT, T., DUVAL, B.P., HOLLENSTEIN, C., JOYE, B., in Controlled Fusion and Plasma Physics (Proc. 17th Europ. Conf., Amsterdam 1990), Vol. 3, European Physical Society (1990) 1476.

[24] TFR GROUP, Nucl. Fus. **27** (1987) 1975.

[25] FOM-ECRH team, Equipe TFR, in Controlled Fusion and Plasma Physics (Proc. 14th Europ. Conf., Madrid 1987), Vol. 3, European Physical Society (1987) 876.

[26] DUDOK DE WIT, T., DUVAL, B.P., JOYE, B., LISTER, J.B., MORET, J.-M., in Controlled Fusion and Plasma Physics (Proc. 16th Europ. Conf., Venice 1989), Vol. 1, European Physical Society (1989) 59.

[27] LJUNG, L., System Identification, Prentice-Hall, London (1987).

APPENDIX : ANALYSIS METHODS

Because of the transitory nature of the experimental plasma signals, particular care must be given to the analysis methods used to obtain the dynamical response. Two techniques have been used on TCA.

1) Sinusoidal response analysis

When a sinusoidal excitation

$$x(t) = Re(\mathbf{X}\, e^{-j\omega t}) = Re(\mathbf{X}) \cos \omega t + Im(\mathbf{X}) \sin \omega t \qquad (A.1)$$

is fed into a linear system, the output is also a sinusoidal signal

$$y(t) = Re(\mathbf{Y}\, e^{-j\omega t}) \qquad (A.2)$$

from which the transfer function at the chosen frequency

$$H(\omega) = \frac{\mathbf{Y}}{\mathbf{X}} \qquad (A.3)$$

may be obtained. The common techniques for extracting H are standard Fourier analysis or cross-correlation between input and output. However, these techniques require an integer number of cycles to be analysed, and need adequate prefiltering of the signals in order to remove drifts and offsets. An alternative to this is a least square fit which includes sinusoidal terms and explicit offset and linear drift terms

$$\hat{y}(t') = Re\left(\hat{\mathbf{Y}}(t)\right) \cos \omega t' + Im\left(\hat{\mathbf{Y}}(t)\right) \sin \omega t' + \langle y \rangle(t) + \frac{d\langle y \rangle(t)}{dt} (t'-t) \qquad (A.4)$$

This fit may be performed in a time window of arbitrary width $|t-t'| \geq \Delta T/2$, in which the parameters $\langle y \rangle$ and $d\langle y \rangle/dt$ are taken to be constant. Applying a standard Fourier analysis when the window contains a non integer or a finite number of cycles yields biased estimators of the parameters while it is not the case with this least square fit. A temporal resolution ΔT of the order of or smaller than the modulation period can be achieved.

This method can also be extended to several sinusoidals, or include a quadratic

drift correction. The latter was not necessary in our experiments.

2) System identification

The drawback of the sinusoidal methods is their need for a well defined excitation signal. For more complex stimuli, such as a gas puff or an impurity injection pulse, a method based on parametric system identification is necessary.

This method makes use of the z transform, which is the equivalent of the Laplace transform for discretly time sampled signals. For a large class of linear systems, the stimulus and the response satisfy an N^{th} order linear differential equation

$$\sum_{n=0}^{N} \alpha_n \frac{d^n y(t)}{dt^n} = \sum_{m=0}^{M} \beta_m \frac{d^m x(t)}{dt^m} \qquad (A.5)$$

in which the parameters α and β completely describe the physical characteristics of the system. The Laplace transform of (A.5) gives

$$\sum_{n=0}^{N} \alpha_n s^n y(s) = \sum_{m=0}^{M} \beta_m s^m x(s) \qquad (A.6)$$

from which the transfer function expressed in the Laplace variable is derived

$$H(s) = \frac{y(s)}{x(s)} = \frac{\sum_{m=0}^{M} \beta_m s^m}{\sum_{n=0}^{N} \alpha_n s^n} \qquad (A.7)$$

The z-transform of a signal u which is sampled at a constant period T is defined by

$$\mathcal{Z}(u(k)) = u(z) = \sum_{k=-\infty}^{+\infty} u(k)\, z^{-k} \qquad (A.8)$$

where it may be shown that $u(s) = u(z=e^{sT})$. The z-transform may be directly used to express delays

$$\mathcal{Z}(u(k-1)) = z^{-1}\, \mathcal{Z}(u(k)) \qquad (A.9)$$

which may be written $z^{-1}\, u(k) = u(k-1)$. For frequencies much smaller than the

Nyquist frequency ($\omega << \pi/T$) the bilinear mapping approximation may be used

$$s = \frac{2}{T}\frac{1-z^{-1}}{1+z^{-1}} \tag{A.10}$$

The transfer function (A.7) can then be expressed as a rational fraction of polynomials in z^{-1}

$$H(z) = \frac{\sum_{m=0}^{N} b_m z^{-m}}{\sum_{n=0}^{N} a_n z^{-n}} \tag{A.11}$$

Applying this transfer function to the sampled input x(k) directly yields the sampled output y(k)

$$y(k) = \sum_{m=0}^{M} b_m\, x(k-m) - \sum_{n=1}^{N} a_n\, y(k-n) \tag{A.12}$$

where both polynomials have been normalised by a_o.

The polynomial coefficients a_n and b_m may be estimated by minimising the difference between the estimated output given by (A.12) and the data for which several optimisation techniques are available [27]. Once the polynomial coefficients are known, an inverse bilinear mapping can be used to return to the Laplace and frequency domains and estimate the transfer function for frequencies up to π/T.

In our case where the electron temperature and density are governed by partial differential equations differing from Eq. (A.5), the z-transform analysis cannot be strictly applied. However, each temperature response along a given chord can still be satisfactorily modelled, provided that the order N of the system is increased. In practice, an excellent modelling of the temperature evolution is already obtained for N= 2 to 4.

FIGURE CAPTIONS

1 a) Raw soft X-ray traces during sinusoidal gas feed modulation at 100 Hz. b) The relative modulated component $\tilde{A}$. In both figures, a common scale is used for all signals.

2 Relative gain and phase profiles of the emission response to the line-averaged density during gas feed modulation at 100 Hz, for two plasma currents.

3 Contour plot of the phase response of the emission during RF power modulation, with a range of plasma currents. Also shown is the position of the sawtooth inversion radius (filled circles) and the position of the q=1 radius (open circles) measured by phase contrast interferometry .

4 Temporal evolution of the raw Soft X-ray emission following a) A short gas puff, b) Aluminium injection (the injection time is marked by an arrow), c) An RF power pulse.

5 Dynamical response of the emission to RF power modulation, at two modulation frequencies. The relative amplitude and phase profiles associated with the sawtooth propagation at f=1100 Hz are shown for comparison, with an arbitrary phase reference.

6 Comparison of the relative gain and phase profiles of the emission response to RF power modulation and to gas feed modulation. The phase reference is the modulated line-averaged density.

7 Comparison of the relative amplitudes of the central emission and of the line-averaged electron density for different stimuli and for different plasma currents.

8 Modification of the relative gain and the phase profiles of the emission caused by a change in the Alfvén resonance structure. Before the arrival of a new resonance layer, all the resonances are situated near the edge. A small increase in the RF frequency brings a new layer into the centre of the plasma, which modifies the dynamical response.

9 Relative gain and phase profiles of the emission normalised with respect to the line-averaged electron density modulation (f=100 Hz), obtained

with RF power modulation. The conditions are : a standard plasma (dots), a plasma with low impurity content (circles) and a plasma with low impurity content and RF power and gas feed countermodulation (triangles).

10 Phase profiles associated with the response of the emission to an injection of aluminium. Three different frequencies are shown. The phase reference is given by the impurity injection pulse.

11 Phase response of the emission to a modulation of the surface loop voltage at f=150 Hz for two different plasma currents, showing the existence of an inward propagating perturbation.

12 Simulation of the heat perturbations generated by current profile changes. The gradient of the temperature phase profile at mid-radius is plotted as a function of the heat diffusion coefficient for three current profiles. Also shown is the gradient which would be obtained for pure heat diffusion i.e. without current diffusion.

13 Comparison of the phase profiles of the emission (solid line) and the electron density (grey line) response to RF power modulation, at three modulation frequencies.

14 Phase response of the emission as a function of the square root of the modulation frequency, at three radial positions : at the centre, at the q=1 radius and near the edge.

15 Simulation of the effect of a local perturbation of the diffusion coefficient. From top to bottom : the unperturbed profile (e.g. the temperature or density); the perturbed diffusion coefficient; the corresponding source dipole and the resulting gain and phase response profiles of the plasma.

16 Profile of the diffusion coefficient required to simulate a response observed on TCA together with the local perturbation on D and the resulting phase response.

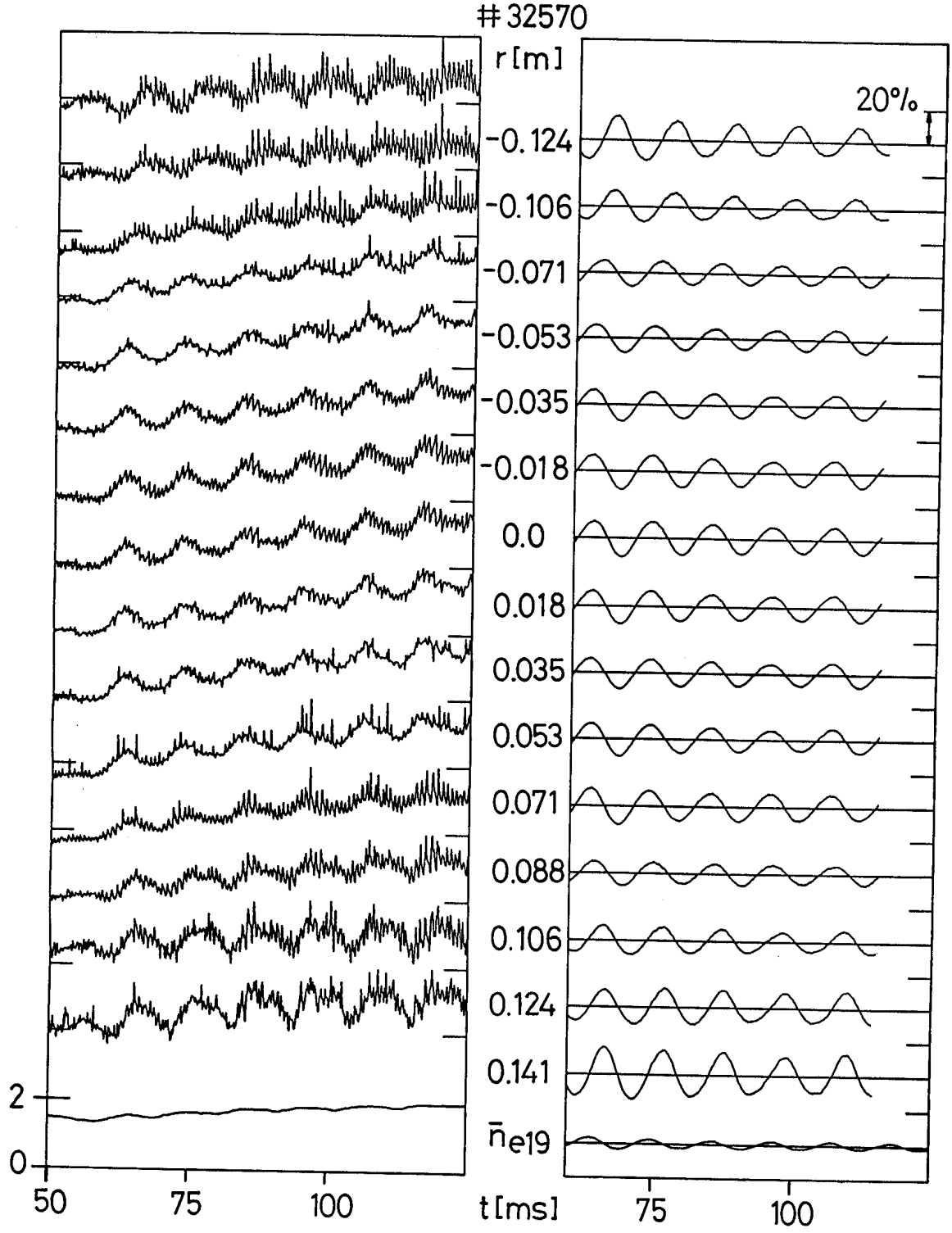
#32570
r[m]
20%
-0.124
-0.106
-0.071
-0.053
-0.035
-0.018
0.0
0.018
0.035
0.053
0.071
0.088
0.106
0.124
0.141
$\bar{n}_{e19}$
2
0
50
75
100
t[ms]
75
100

Figure 1

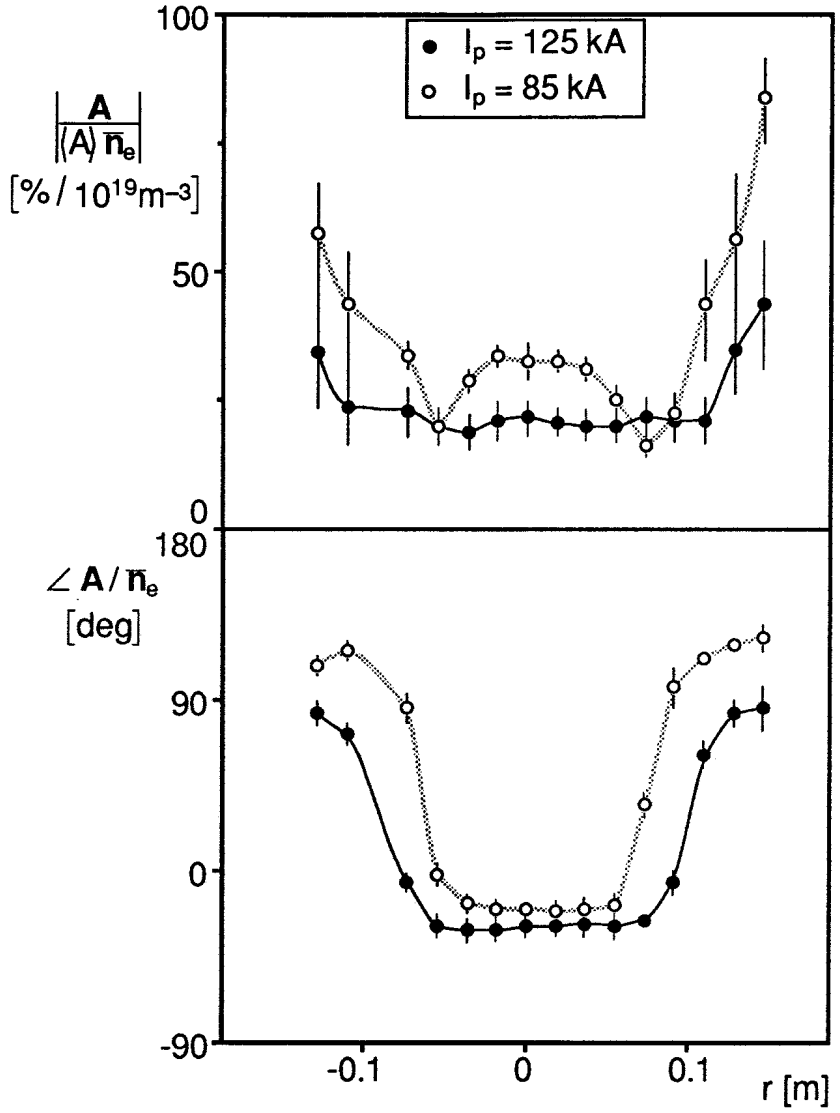

Figure 2

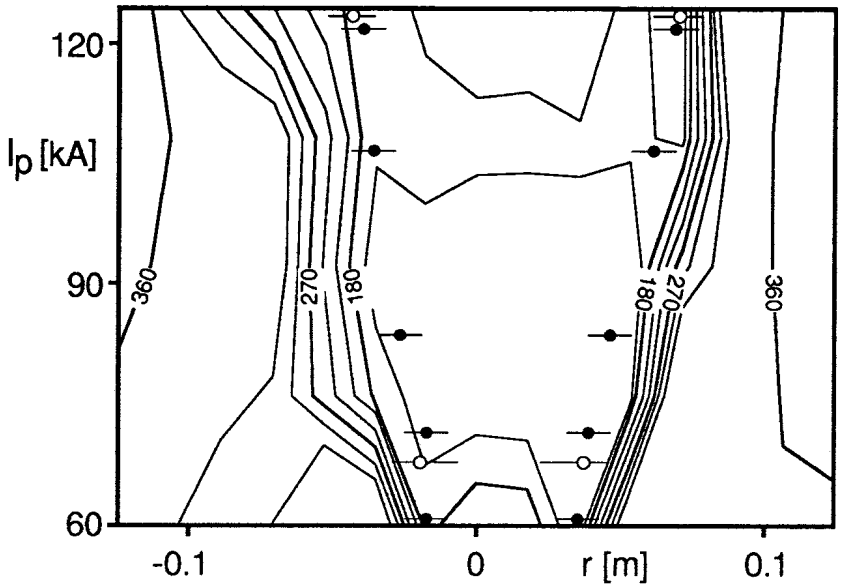

Figure 3

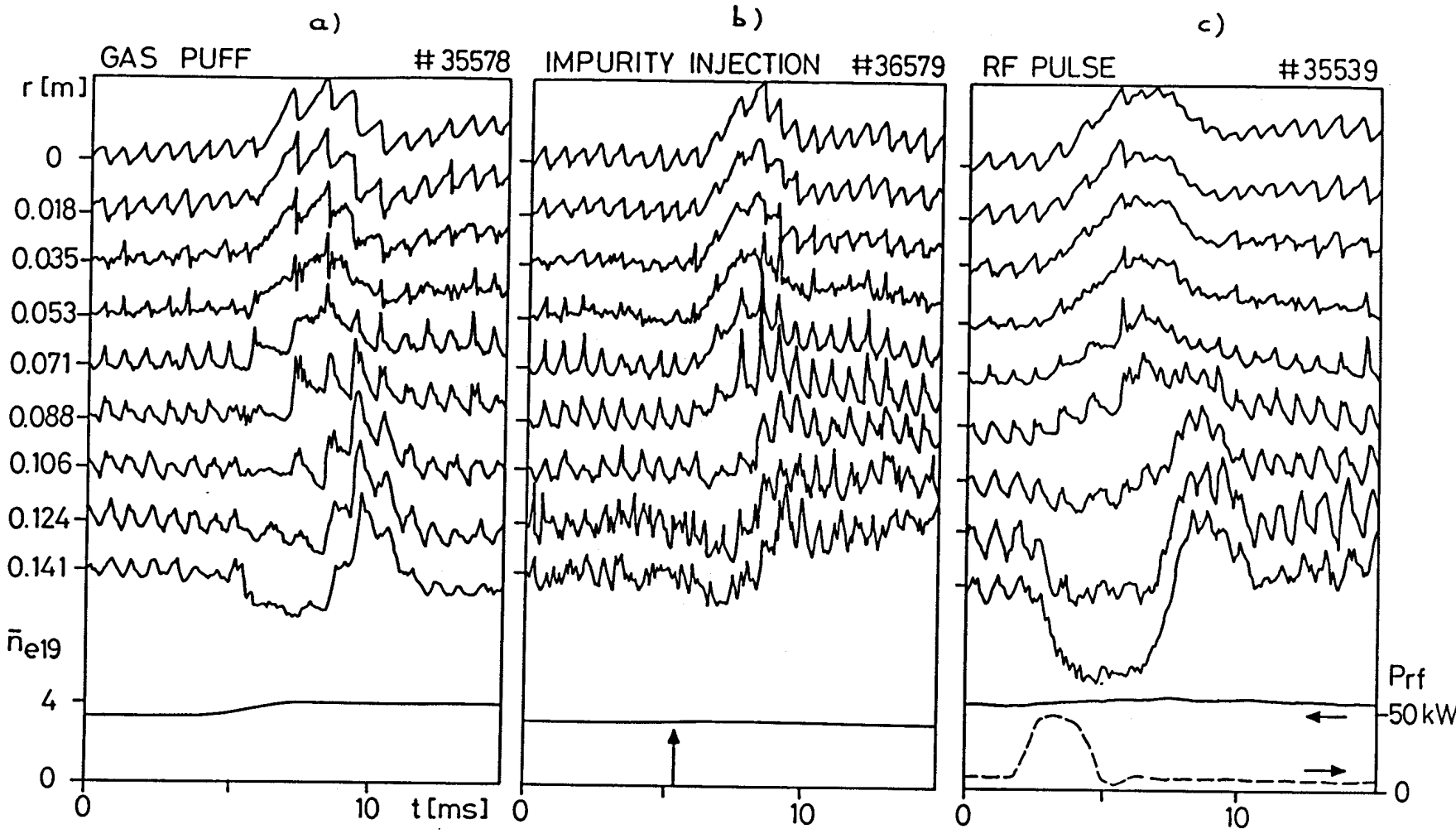
a)
GAS PUFF
#35578
b)
IMPURITY INJECTION
#36579
c)
RF PULSE
#35539
r [m]
0
0.018
0.035
0.053
0.071
0.088
0.106
0.124
0.141
$\bar{n}_{e19}$
4
0
0
10
t [ms]
0
10
0
10
Prf
50 kW
0

Figure 4

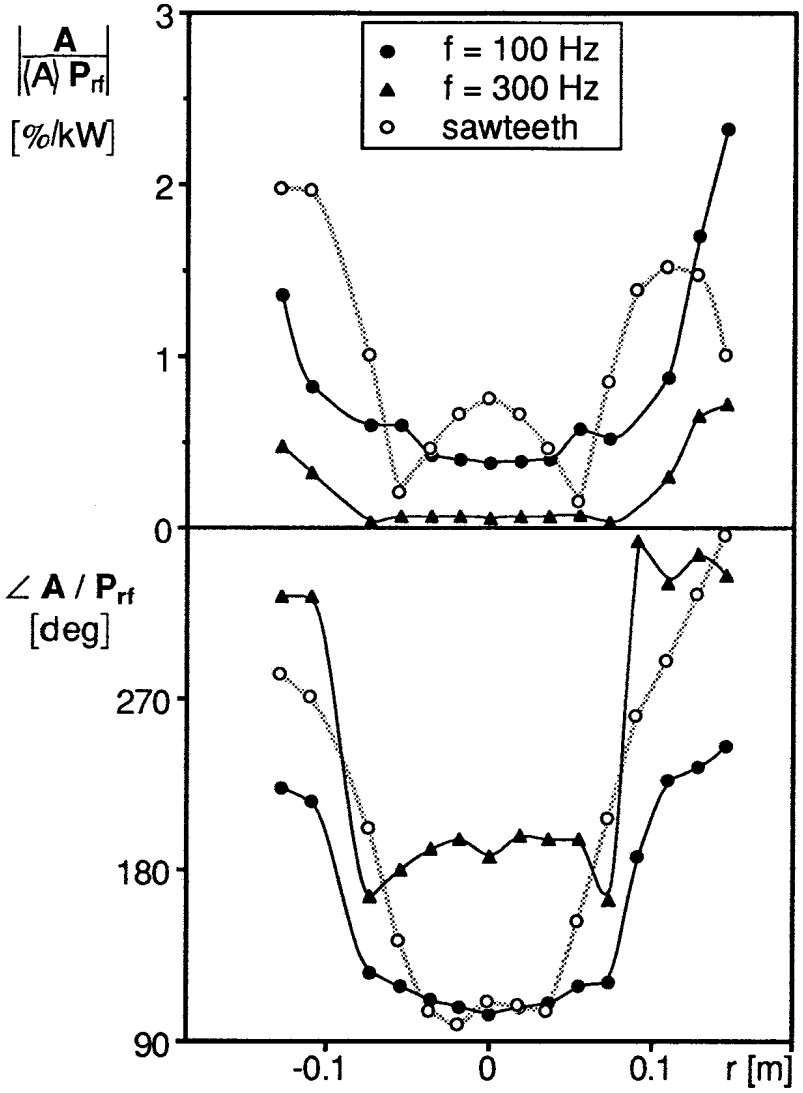

Figure 5

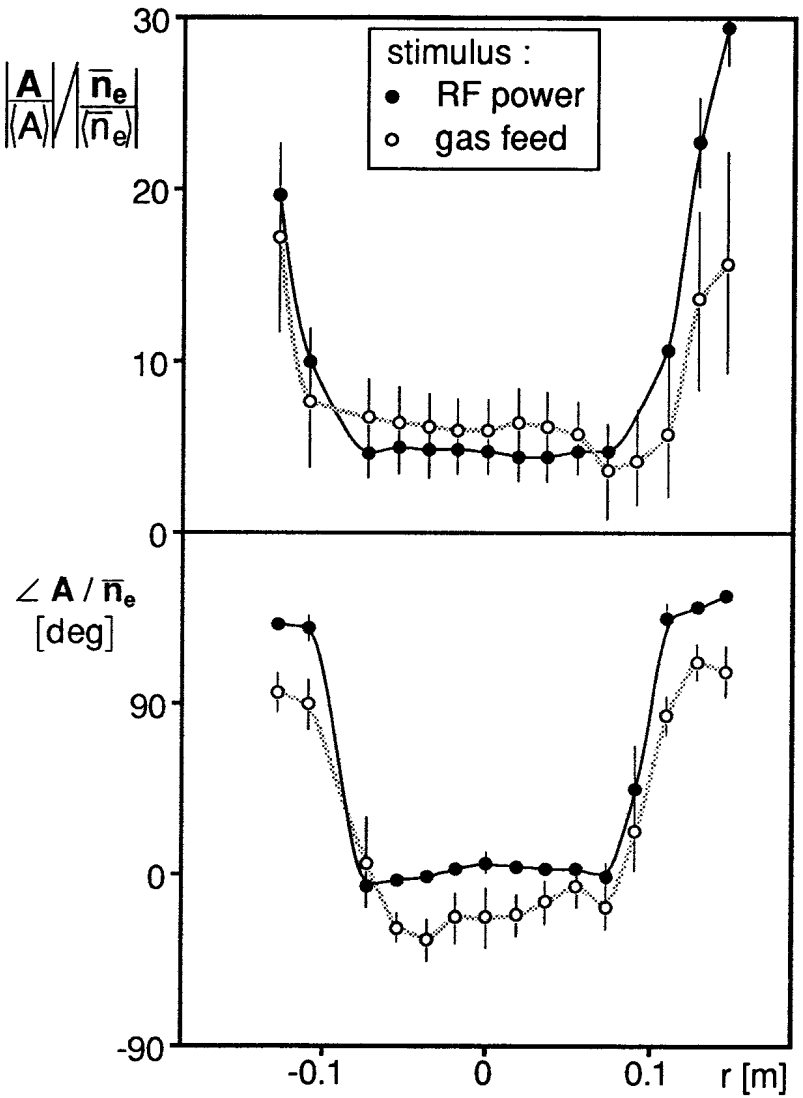

Figure 6

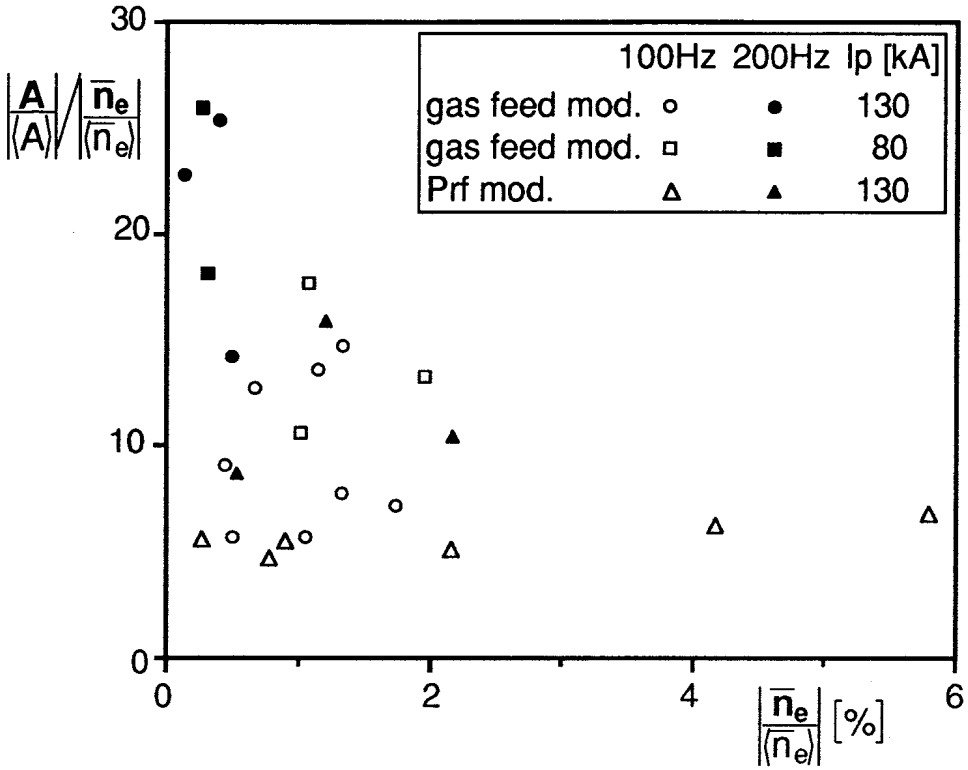

Figure 7

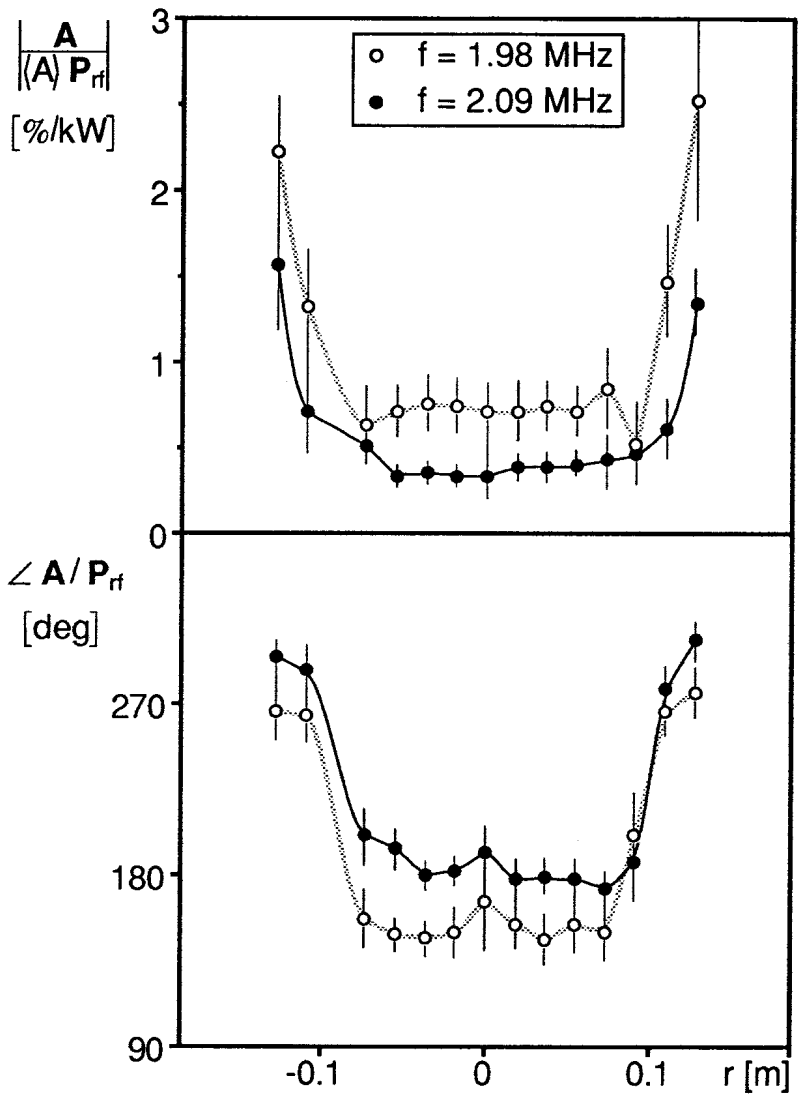

Figure 8

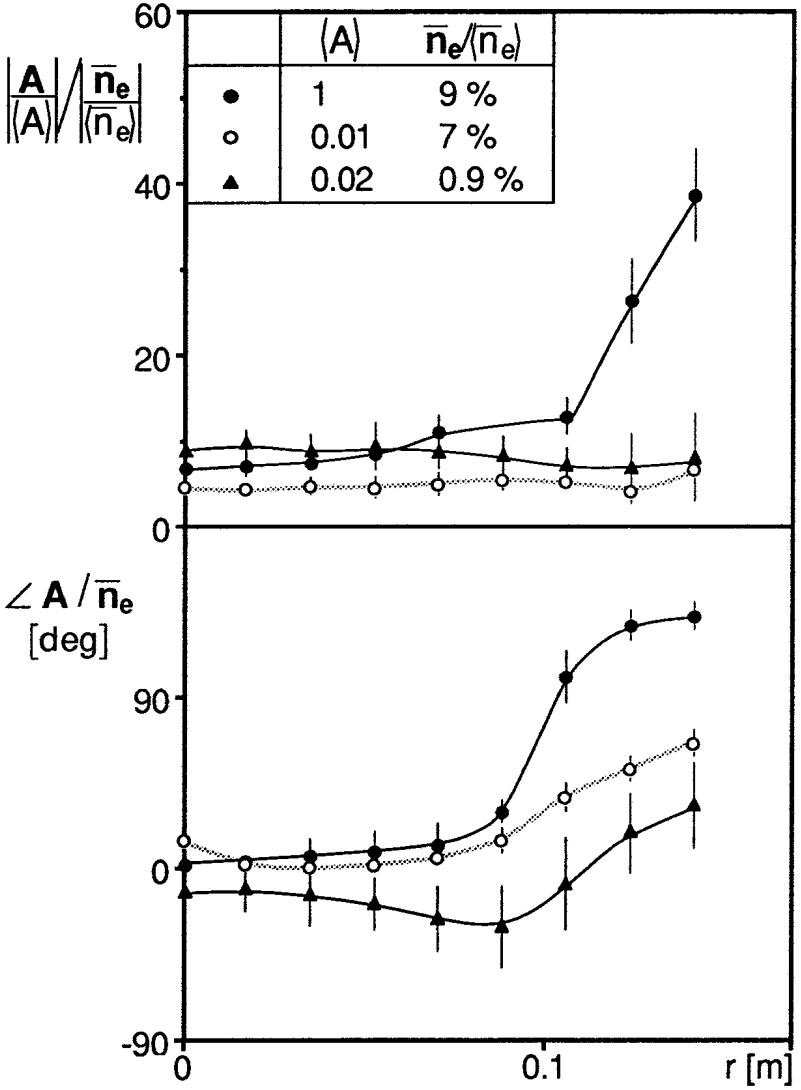

Figure 9

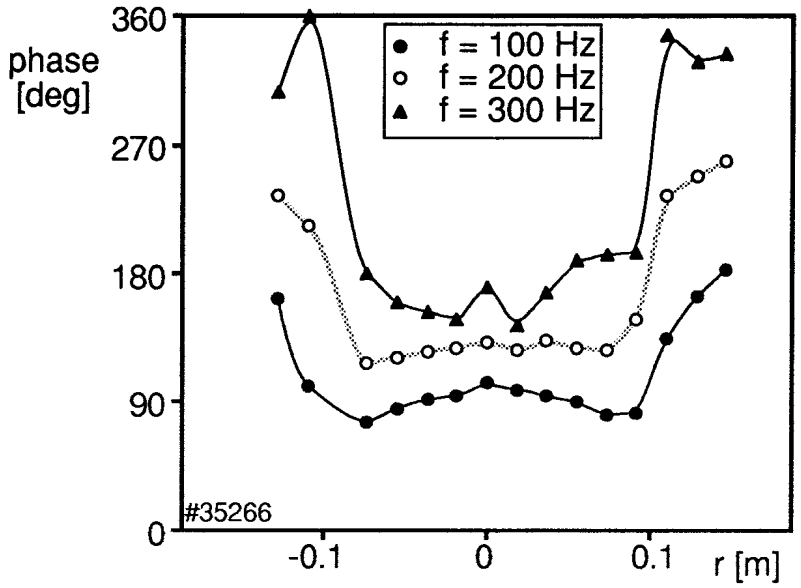

Figure 10

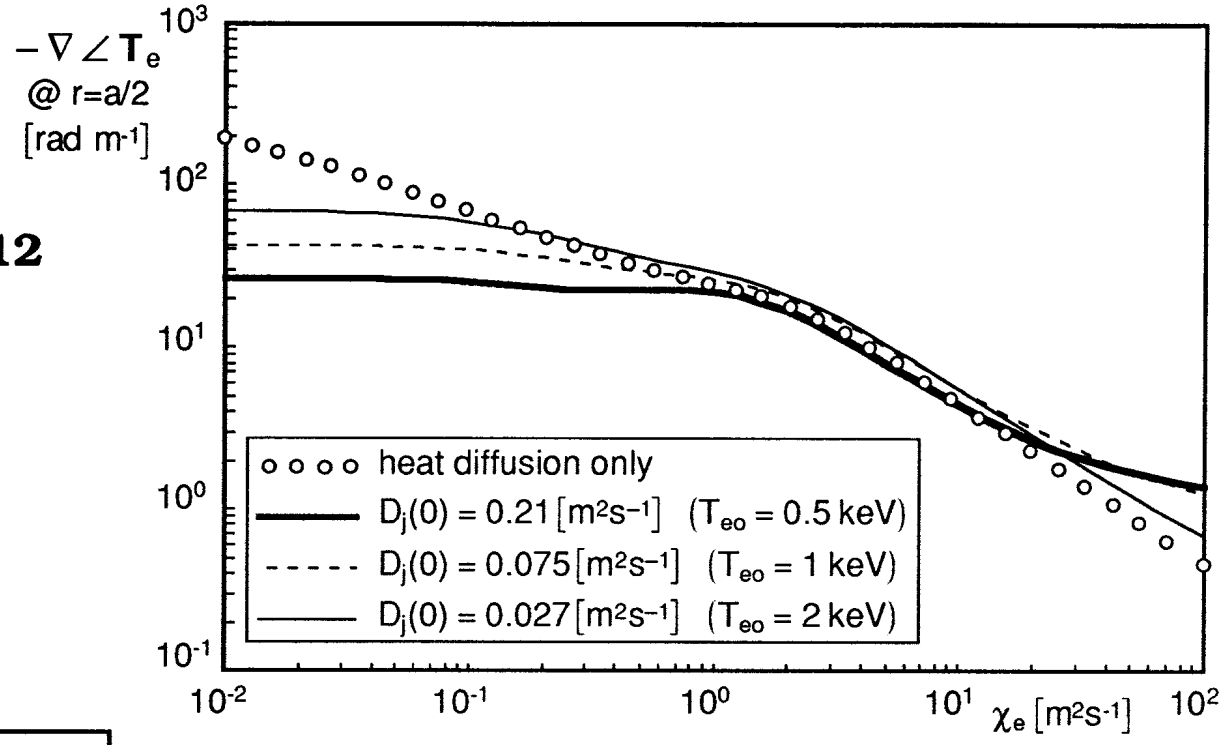

Figure 12

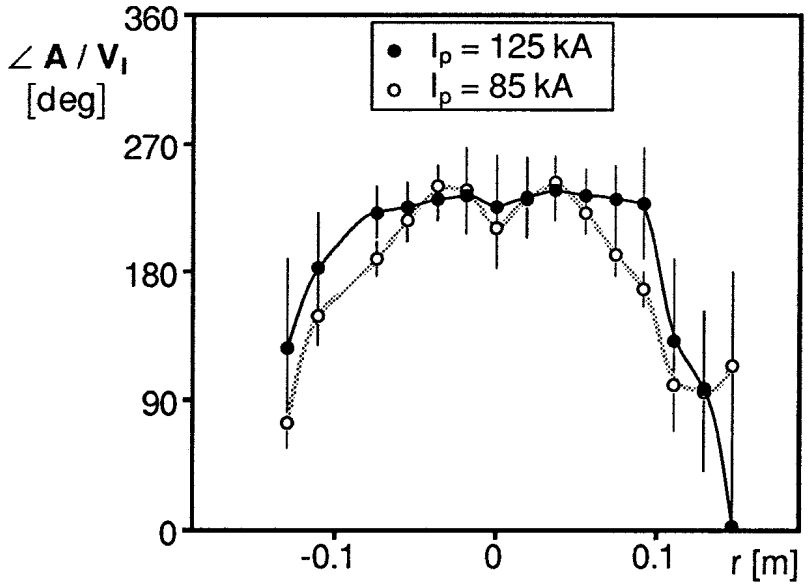

Figure 11

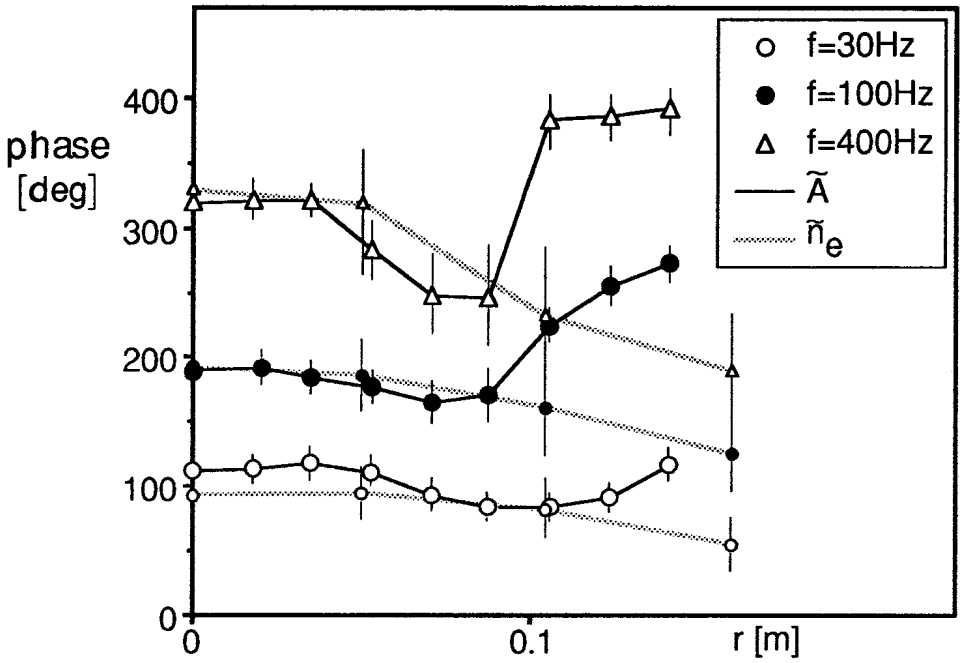

Figure 13

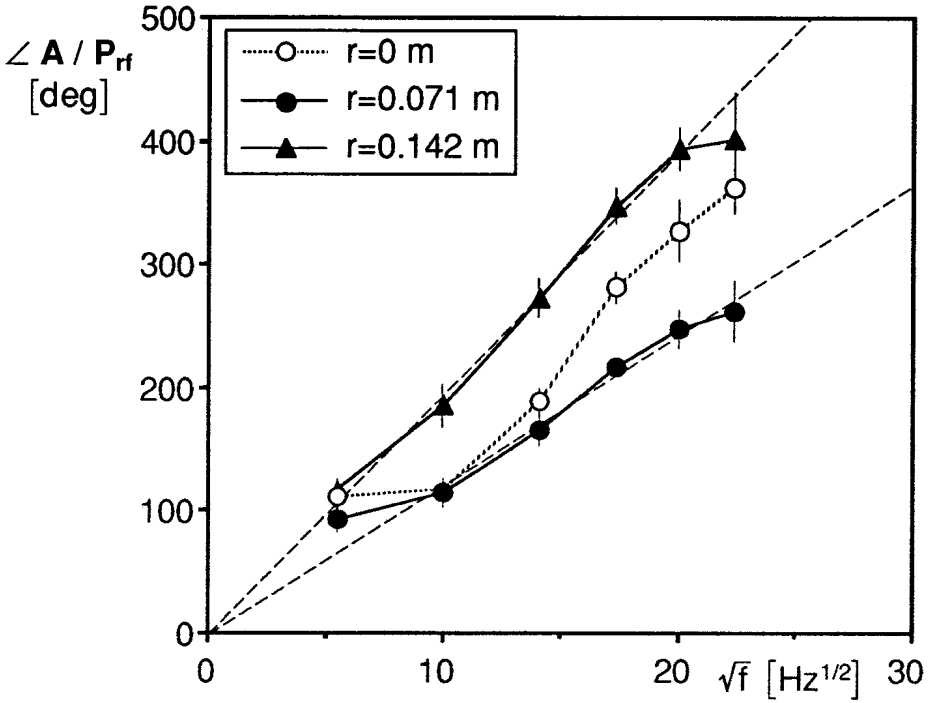

Figure 14

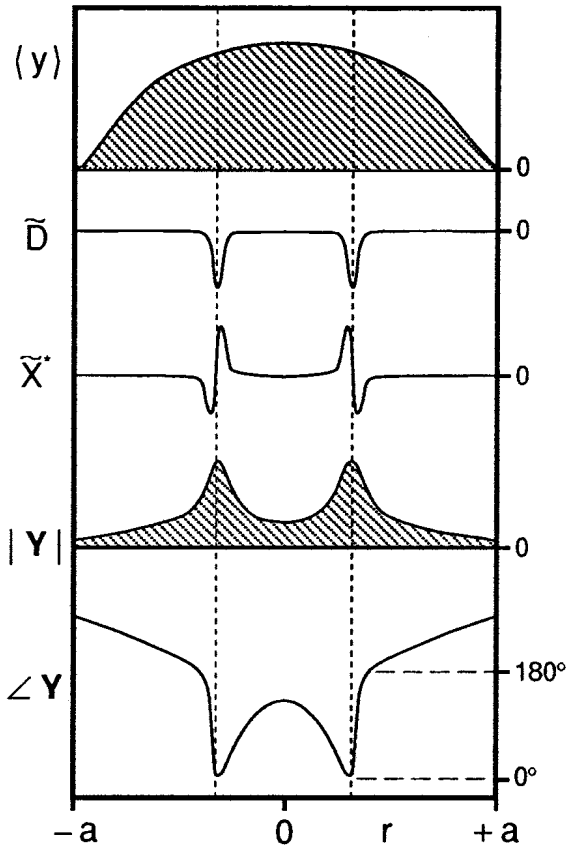

Figure 15

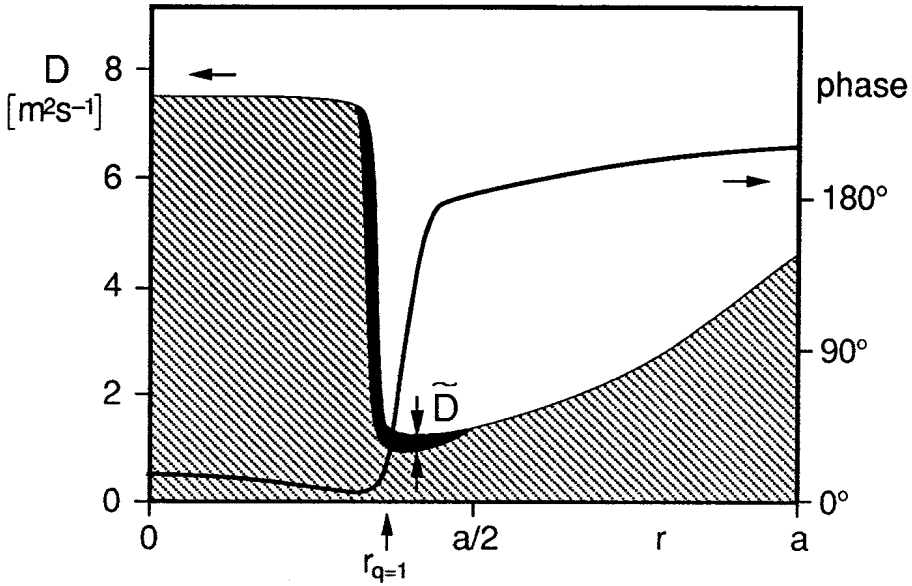

Figure 16